Journal of Magnetic Resonance 203 (2010) 274–282

Contents lists available at ScienceDirect

Journal of Magnetic Resonance

journal homepage: www.elsevier.com/locate/jmr

Operation of a 500 MHz high temperature superconducting NMR: Towards an NMR spectrometer operating beyond 1 GHz

Y. Yanagisawa [a,b], H. Nakagome [b], K. Tennmei [c], M. Hamada [d], M. Yoshikawa [e], A. Otsuka [e], M. Hosono [f], T. Kiyoshi [g], M. Takahashi [a,c], T. Yamazaki [a], H. Maeda [a,c,*]

[a] Systems and Structural Biology Center, RIKEN, Yokohama 230-0045, Japan
[b] Graduate School of Engineering, Chiba University, Chiba 236-8522, Japan
[c] Graduate School of Yokohama City University, Yokohama 230-0045, Japan
[d] Kobe Steel, Ltd., Kobe, Hyogo 651-2271, Japan
[e] Japan Superconductor Technology, Inc., Kobe, Hyogo 651-2271, Japan
[f] JEOL, Akishima, Tokyo 196-8558, Japan
[g] Superconducting Materials Center, National Institute for Materials Science, Tsukuba 305-0003, Japan

ARTICLE INFO

Article history:
Received 15 October 2009
Revised 14 January 2010
Available online 18 January 2010

Keywords:
Ultra high magnetic field NMR
High temperature superconductor
Bi-2223
External current mode
Field fluctuation
Screening current-induced magnetic field
Internal deuterium lock
NOESY
HNCO
HNCACB

ABSTRACT

We have begun a project to develop an NMR spectrometer that operates at frequencies beyond 1 GHz (magnetic field strength in excess of 23.5 T) using a high temperature superconductor (HTS) innermost coil. As the first step, we developed a 500 MHz NMR with a Bi-2223 HTS innermost coil, which was operated in external current mode. The temporal magnetic field change of the NMR magnet after the coil charge was dominated by (i) the field fluctuation due to a DC power supply and (ii) relaxation in the screening current in the HTS tape conductor; effect (i) was stabilized by the ^{2}H field-frequency lock system, while effect (ii) decreased with time due to relaxation of the screening current induced in the HTS coil and reached 10^{-8}(0.01 ppm)/h on the 20th day after the coil charge, which was as small as the persistent current mode of the NMR magnet. The 1D ^{1}H NMR spectra obtained by the 500 MHz LTS/HTS magnet were nearly equivalent to those obtained by the LTS NMR magnet. The 2D-NOESY, 3D-HNCO and 3D-HNCACB spectra were achieved for ubiquitin by the 500 MHz LTS/HTS magnet; their quality was closely equivalent to that achieved by a conventional LTS NMR. Based on the results of numerical simulation, the effects of screening current-induced magnetic field changes are predicted to be harmless for the 1.03 GHz NMR magnet system.

1. Introduction

Nuclear magnetic resonance (NMR) is widely used in biology, organic chemistry, and material science [1]. As both the NMR sensitivity and the NMR signal resolution improve with increasing magnetic field strength, NMR spectroscopists pursue higher magnetic fields for NMR spectrometers [2,3]. A field of 23.5 T, allowing NMR operation at 1 GHz, has already been achieved by using low temperature superconductors (LTS) such as NbTi and Nb_3Sn [4]. However, the critical current density for Nb_3Sn decreases steeply as the magnetic field strength exceeds 23 T, and therefore it is improbable that LTS NMR magnet operation can substantially exceed 1 GHz, although fields allowing operation at slightly >1 GHz are likely to be feasible if we could take advantage of a restacked rod process (RRP) Nb_3Sn or Nb_3Al [5,6]. On the contrary, if we use magnets of high temperature superconductor (HTS) such as $Bi_2Sr_2Ca_2Cu_3O_x$ (Bi-2223) [7], $Bi_2Sr_2CaCu_2O_x$ [8] and $YBa_2Cu_3O_x$ [9], sufficiently high current density is available above 1 GHz (23.5 T), enabling an NMR to substantially exceed 1 GHz (23.5 T), such as 1.3 GHz (30.53 T), by using HTS materials.

Thus, we have started a project to develop an NMR spectrometer that may be operated at frequencies of 1.03 GHz (magnetic field strength 24.2 T) by using an innermost coil made of the Bi-2223 HTS coil [10,11]; this is a first step towards an NMR spectrometer operated at substantially beyond 1 GHz. The project consists of two programs. The first program is to develop a LTS/HTS 500 MHz NMR spectrometer to investigate the basic behavior of the LTS/HTS NMR spectrometer; the LTS/HTS NMR coil consists of a low-field LTS coil and a high-field HTS coil. The second program has the goal of developing a LTS/HTS 1.03 GHz NMR spectrometer. The purpose of this paper is to describe the experimental results from the first program.

The LTS NMR magnet is usually operated in persistent current mode with a decay rate of $<10^{-8}$ (10 ppb)/h. It is stabilized to 10^{-10} (0.1 ppb) by an internal ^{2}H field-frequency lock system

* Corresponding author. Address: Systems and Structural Biology Center, RIKEN, Yokohama 230-0045, Japan. Fax: +81 045 508 7360.
E-mail addresses: maeda@jota.gsc.riken.jp, maeda@jota.gsc.riken.go.jp (H. Maeda).

1090-7807/$ - see front matter © 2010 Elsevier Inc. All rights reserved.
doi:10.1016/j.jmr.2010.01.007

installed in the NMR spectrometer [11]. Due to the low n-index value of the Bi-2223 HTS tape conductor [12] and the difficulty in guaranteeing a superconducting joint, a Bi-2223 HTS coil is unlikely to provide a persistent current sufficient for NMR measurement. Therefore, the LTS/HTS NMR magnet is driven by an external DC power supply. The current fluctuation of the DC power supply causes a field fluctuation, generating noticeable sidebands on the NMR spectrum and a deviation in peak frequency [11]. We have demonstrated that the ^{2}H field-frequency lock system stabilizes the magnetic field fluctuation, if the peak–peak amplitude of the fluctuation is $<3 \times 10^{-6}$ (±1.5 ppm) [11]. Thus, we have developed an ultra-stabilized DC power supply with a current stability of $<10^{-6}$ (1 ppm), so that the field fluctuation caused by the power supply is stabilized by the ^{2}H field-frequency lock system [13]. The effects of the power supply on the spectra are described in this paper.

When the Bi-2223 magnet is charged, a screening current is induced in the Bi-2223 tape conductor, generating an additional central magnetic field as shown by Hahn et al. [14]. Its relaxation results in the positive drift of the central magnetic field with time, after the magnet is charged to the operation current [15]. If the temporal change in the screening current-induced magnetic field exceeds 3×10^{-6} (±1.5 ppm), the field-frequency lock system loses operation and it is impossible to achieve a high resolution NMR spectrum. Thus the effect of screening current-induced magnetic field on the magnetic field stability for the LST/HTS NMR is investigated in this paper and the results will be discussed based on a numerical simulation study.

Hahn et al. [14] achieved a ^{1}H NMR spectrum with an LTS/HTS 700 MHz NMR magnet driven by an external DC power supply. They used neither room temperature shims nor a field-frequency lock system and therefore the half-height line width of the spectrum was as large as ~kHz. The present 500 MHz LTS/HTS NMR spectrometer uses both these features and therefore the resolution and the sensitivity are several orders of magnitude better than those reported by Hahn et al. [14]. The magnetic field stability, line shape, NMR sensitivity and 1D, 2D and 3D NMR spectra on proteins will be used to demonstrate NMR operation in this paper.

2. Experimental procedure

2.1. The Bi-2223 HTS innermost coil

The multi-filamentary Bi-2223 HTS tape used for the innermost coil of the LTS/HTS NMR magnet was 4.55 mm in width and 0.36 mm in thickness, reinforced by copper-alloy tapes soldered on both sides. It was wrapped with Kapton tape for electrical insulation. The Bi-2223 HTS tape was developed by Sumitomo Electric Industries, Ltd. Two winding methods, i.e. double-pancake winding and solenoid winding, may be used for HTS coil fabrication. The double-pancake coil consists of a number of pancakes, each of which resembles a tape recorder spool. From the viewpoint of coil fabrication, the double-pancake method is desirable for a tape of Bi-2223. On the other hand, a solenoid method is preferable from the perspective of magnetic field homogeneity as the coil is tightly wound by the conductor; however, winding a solenoid with Bi-2223 tape is rather difficult as the aspect ratio of the tape is as large as 13. After testing several Bi-2223 model coils, wound by both methods, we decided to employ solenoid winding for the Bi-2223 innermost coil.

The Bi-2223 innermost coil was 81.2 mm in inner diameter, 121 mm in outer diameter, and 375 mm in length. An Nb_3Sn innermost coil from a conventional 600 MHz NMR magnet made by JASTEC was replaced by the Bi-2223 innermost coil. The Bi-2223 HTS coil was designed to generate 1.797 T, while the LTS was capable of 9.947 T at the operation current of 144 A (11.743 T). More details of the design and fabrication of the Bi-2223 coil will be found elsewhere [16].

2.2. Highly stabilized DC power supply

The Bi-2223 HTS coil was connected in series to the LTS backup coil and charged simultaneously by an ultra-stabilized external DC power supply. As described above, the ^{2}H field-frequency lock system stabilized the magnetic field fluctuation with a peak–peak amplitude $<3 \times 10^{-6}$ (±1.5 ppm). We developed a highly stabilized external DC power supply, assisted by Danfysik [17]; its long-term current stability over 8 h was $<10^{-6}$ (1 ppm) with short-term current stability achieving $<5 \times 10^{-7}$ (0.5 ppm). The field fluctuation provided by the DC power supply was therefore assumed to be fully stabilized by the ^{2}H field-frequency lock [11,13].

2.3. Cryostat

The LTS/HTS NMR magnet was operated in liquid helium at 4.2 K. In the external current mode of the NMR magnet, both heat conduction and Joule heating on the current leads increase liquid helium consumption [18]. Thus, an HTS single-crystal bulk rod, with high thermal resistivity, was used as a part of the current lead so that heat leak to the helium bath was suppressed. Secondly, a two stage cryocooler, i.e. a small refrigerator with two cold stages, was installed on top of the cryostat; vaporized helium gas was reliquefied by the second stage of the cryocooler, running at 4 K. The high temperature end of the HTS bulk rod was anchored to the first stage of the cryocooler, at a temperature of 50 K.

Two kinds of cryocooler were employed for the NMR magnet, a Gifford–McMahon (GM) cycle cryocooler and a pulse-tube cryocooler. The advantage of the GM cryocooler is its large cooling capacity, typically 1 W, while it has the disadvantage of inducing mechanical vibration on the magnet due to reciprocating movement of the displacer inside the cryocooler. The pulse-tube cryocooler on the other hand has low levels of mechanical vibration, but offers lower cooling power (0.5 W). Long-term NMR experiments over two months were conducted using each type of cryocooler. Temperatures of the LTS coil, a radiation shield, and the cold stages of the cryocooler were continuously measured over the experiment interval.

2.4. NMR probe and spectrometer

The LTS NMR magnet was originally manufactured for a 600 MHz NMR spectrometer, although we operated it at 500 MHz in this experiment. A commercial 600 MHz triple resonance probe (Bruker) was used for the NMR measurement; its resonance frequency was changed from 600 to 500 MHz. The 500 MHz NMR spectrometer (DMX 500 by Bruker Biospin) was used for NMR measurements; a ^{2}H field-frequency lock system built into the spectrometer was used to stabilize the magnetic field fluctuation caused by the DC power supply, as described below.

3. Experimental results

3.1. Initial change in the magnetic field after charging the NMR magnet

The NMR magnet was charged to 145.000 A (a magnetic field of 11.846 T, corresponding to an operating frequency of 504.352 MHz), and was operated in external current mode. Fig. 1 (black-solid line) shows the initial change in the magnetic field intensity with time measured by an NMR meter (Model PT 2025, Metrolab

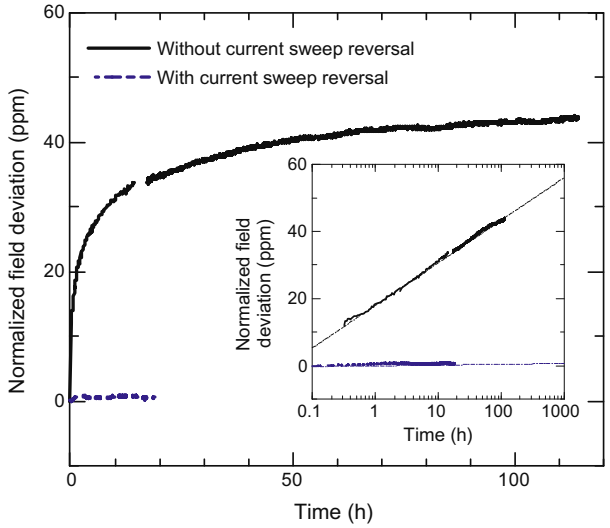

Fig. 1. Positive drift of the central magnetic intensity with time after charging the magnet to the operation current at $t = 0$ h; the time dependent component of the central magnetic field is shown in the figure, which is normalized to the NMR magnetic field strength. The magnetic field intensity increased with time with a rate of increase that dropped rapidly with time. If we used a current sweep reversal technique, the initial magnetic field drift was stabilized as shown by the blue broken line and the magnetic field became nearly constant just after the coil charge. Inset: Magnetic field deviation vs. logarithmic time.

Instruments); note that the vertical axis is normalized to the NMR operation field. After attaining the operation current at $t = 0$ h, the magnetic field intensity increased with time at a rate of 1.9×10^{-5} (19 ppm)/h at first, and then tended to saturate at 5×10^{-8}/h (50 ppb/h) at $t = 110$ h. Screening current was induced in the Bi-2223 tape by the radial component of the NMR magnetic field, generating a negative central magnetic field at the coil center [15]. Relaxation of the screening current resulted in positive drift of the magnetic field intensity as seen in Fig. 1. As the field drift was due to flux creep on the Bi-2223 tape [15], the magnetic field intensity seen in the inset of Fig. 1 varied linearly with logarithmic time [15,19]. More detail discussion of this observation will be given below. At $t = 150$ h, the magnet current was rearranged to 143.725 A, resulting in 11.743 T and 499.971 MHz operation.

3.2. Magnetic field instability in external current mode

Fig. 2 shows a magnetic field fluctuation on the 20th day ($t = 480$ h) after the magnet charge; the magnetic field is determined by a peak picking process of the $CHCl_3$/acetone-d6 spectra. The vertical axis is normalized to the NMR operation field. The field fluctuation consisted of three components:

(a) Long-term field drift at a rate of 1×10^{-8} (0.01 ppm)/h, which coincides with the extrapolated value of the line seen in the inset of Fig. 1; i.e. it is due to the screening current-induced magnetic field in the Bi-2223 coil.
(b) Variations in the magnetic field with a time interval ~20 h; the field's peak–peak amplitude was 4×10^{-7} (0.4 ppm). These variations were due to daily changes in the environmental temperatures of the DC power supply, resulting in changes to the coil current.
(c) Short-term field ripples with a peak–peak amplitude $<2 \times 10^{-7}$ (0.2 ppm) and a time interval of 10 min; these fluctuations were due to short-term current ripples caused by the DC power supply.

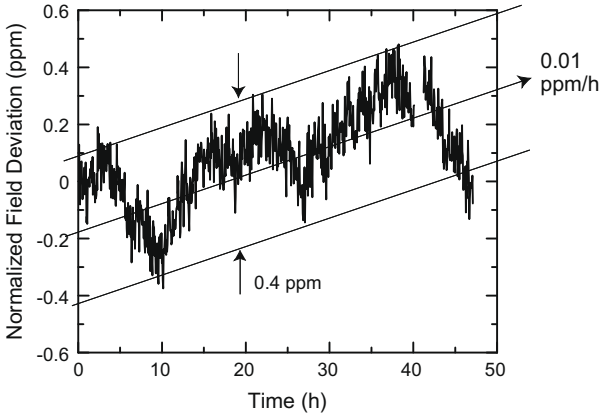

Fig. 2. Magnetic field deviation on the 20th day after the coil charge; it is normalized to the NMR magnetic field strength. The average magnetic field drift was 1×10^{-8}/h; the fluctuations with a peak–peak amplitude of 4×10^{-7} were due to daily temperature changes affecting the DC power supply. Field ripples with a peak–peak amplitude <0.2 ppm were due to short-term current ripples of the DC power supply.

3.3. Field stabilization by the ^2H field-frequency lock operation

Long-term field stability over 74 h with ^2H field-frequency lock operation is shown in Fig. 3 for 1% $CHCl_3$ in acetone-d6; the magnetic field was continuously corrected by the z and z^2 shims by using autoshim feature of the NMR spectrometer [20]. As seen in Fig. 3, total change in peak chemical shift over 74 h was as small as 0.25 Hz, corresponding to 5×10^{-10} (0.5 ppb). Although this value is several times higher than that for the LTS NMR spectrometer, i.e. $<10^{-10}$ (0.1 ppb), it is sufficient for high resolution NMR measurement such as of proteins. The half-height line width at $t = 0$ h seen in Fig. 3 was 0.67 Hz, i.e. 1.3×10^{-9} (1.3 ppb), which finally became 0.95 Hz, 1.9×10^{-9} (1.9 ppb) at $t = 74$ h. After the measurement, we improved the line shape by room temperature shims and the initial line shape was recovered by a y shim; i.e. the slight lineshape deterioration seen in Fig. 3 at $t = 74$ h is due to growth of a radial field gradient of y. Temporal change in z and z^2 shim currents during the NMR measurement will be discussed in the next chapter.

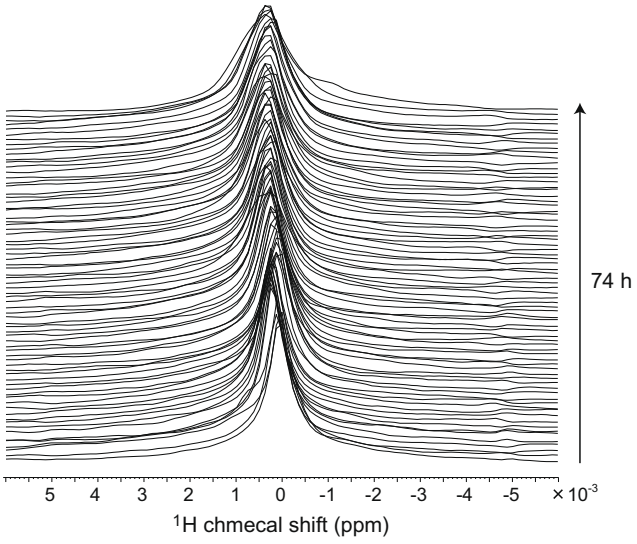

Fig. 3. Stability of the NMR peak frequencies under operation of a ^2H field-frequency lock and auto shimming for z^1 and z^2. The sample was 1% $CHCl_3$ in acetone-d_6. Each spectrum was obtained by a single scan. Spectrum is plotted every 1 h.

3.4. Quality of the NMR spectra

Fig. 4 illustrates the ^{1}H NMR line shape obtained for 1% $CHCL_3$ in acetone-d_6: Fig. 4(a) is the line shape obtained under GM-cycle cryocooler operation; Fig. 4(b) the line shape under pulse-tube cryocooler operation; and Fig. 4(c) the line shape without cryocooler operation. Each spectrum was obtained by a single scan. The line shape for Fig. 4(a) is 0.61, 8.7, and <30 Hz respectively; side bands at 20 Hz are due to sample rotation. They are close to the line shape obtained in persistent current mode, although many sidebands such as 5, 10, 25–35, 50, and 100 Hz appear, due to mechanical vibration induced by the cryocooler. We measured mechanical vibration of the NMR magnet by using an accelerometer [21] attached to the magnet. The observed mechanical resonance frequencies of the magnet system agreed with the sideband frequencies seen in Fig. 4(a). The number of sidebands was definitely reduced when we used a pulse-tube cryocooler, which induced less mechanical vibration on the magnet system, though the sidebands at several Hz and 50 Hz remained, as seen in Fig. 4(b). The sidebands nearly disappeared if we did not operate a cryocooler as shown in Fig. 4 (c); thus it is clear that most of the sidebands seen in Fig. 4(a) and (b) are due to mechanical vibrations induced by the cryocooler.

The DC power supply generated faster fluctuation at 0.02, 1–2, and 50 Hz [11]. A ^{2}H field-frequency lock system could not stabilize 50 Hz ripples while the 0.02 and 1–2 Hz ripples were stabilized. However, the effect of the 50 Hz fluctuation on the NMR spectrum was small, as seen in Fig. 4(c), as the amplitude of the current ripple of the DC power supply at 50 Hz was as small as on the order of 10^{-10} [11].

Fig. 5(a) and (b) shows the ^{1}H sensitivity test results for 0.1% ethylbenzene in $CHCL_3$ obtained using a 500 MHz LTS NMR magnet and a 500 MHz LTS/HTS NMR magnet, respectively. The spectrum was obtained by a single scan with sample rotation of 20 Hz. The sensitivity is determined by the ratio of the central peak height of the quartet at 2.7 ppm to the noise over 0.4 ppm; it is 512 under pulse-tube cryocooler operation. Note that the probe sensitivity for a conventional 500 MHz LTS NMR was 599. The NMR sensitivity for the LTS/HTS NMR magnet was 15% less than that for the LTS NMR magnet; this is due to slight line broadening due to larger field inhomogeneity for the LTS/HTS NMR magnet. In the case of the LTS/HTS NMR magnet, we could not operate a gradient-shim device as the magnetic field fluctuates continuously and therefore the field homogeneity attained by the 500 MHz LTS/HTS NMR was less than that by a 500 MHz LTS NMR.

Fig. 6(a) illustrates the 2D-WATERGATE NOESY spectrum for 2 mM ^{13}C- and ^{15}N-labeled chlorella ubiquitin in 90% H_2O and 10% D_2O obtained using a 500 MHz conventional LTS NMR magnet, while Fig. 6(b) shows that for the 500 MHz LTS/HTS NMR magnet. The water signal at 4.7 ppm in Fig. 6(b) is sufficiently suppressed, though it is slightly broader than that for the 500 MHz LTS NMR seen in Fig. 6(a). Several peaks disappear in Fig. 6(b) compared with Fig. 6(a); the corresponding peaks are indicated by the dashed circle in Fig. 6(a). However they appear if we lower the 2D NMR contour threshold, i.e. signal intensity for the LTS/HTS NMR magnet is lower than that for a LTS NMR magnet. If there is magnetic field instability with time, noticeable t_1 noise will appear along the t_1 axis. The t_1 noise for the LTS/HTS NMR seen in Fig. 6(b) is slightly greater than that for the LTS NMR seen in Fig. 6(a), suggesting larger field instability for the HTS/LTS NMR. However, it is unlikely that we can make an exact comparison, including that for t_1 noise, between the two NOESY spectra seen in Fig. 6, as we used different NMR magnets. Thus, it is demonstrated that quality of the 2D-NOESY spectrum obtained by the 500 MHz LTS/HTS NMR magnet operated in external current mode is nearly equivalent to that obtained by the 500 MHz LTS magnet.

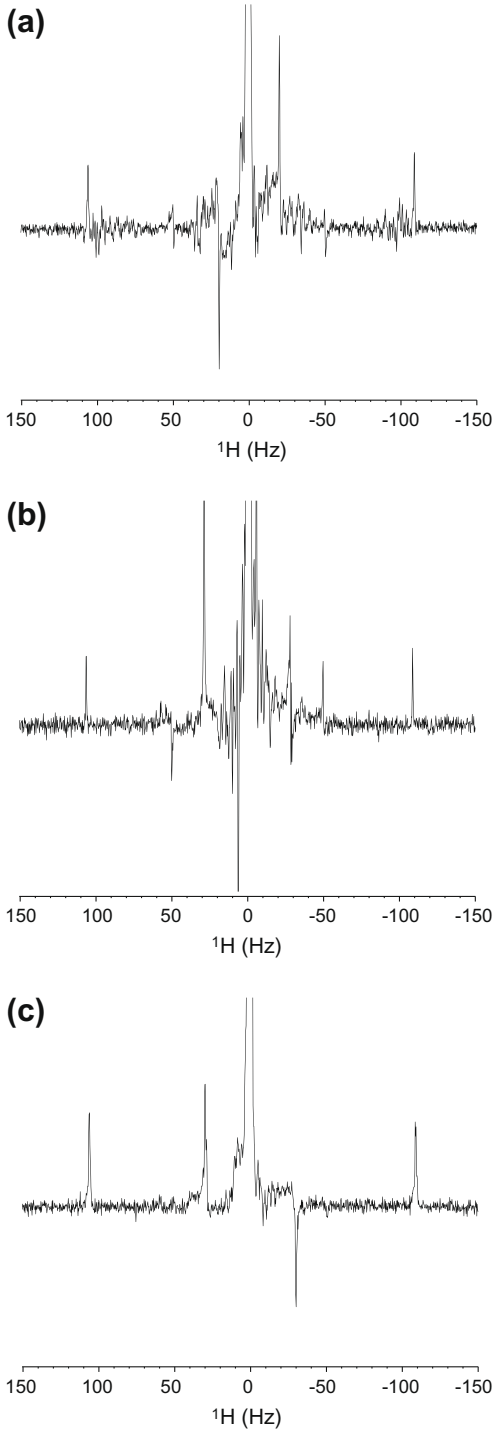

Fig. 4. ^{1}H line shape for 1% chloroform in acetone-d_6 obtained by a single scan. (a) Spectrum obtained under operation of the GM-cycle cryocooler. (b) Spectrum obtained under operation of the pulse-tube cryocooler. (c) Spectrum obtained without cryocooler.

Fig. 7(a) shows the 3D-HNCACB spectrum for 2 mM ^{13}C- and ^{15}N-labeled chlorella ubiquitin in 90% H_2O and 10% D_2O obtained by a 500 MHz LTS NMR magnet, while Fig. 7(b) shows a projection of the spectrum from the ^{13}C–^{1}H aspect. Fig. 7(c) shows the 3D-HNCACB spectrum obtained by the 500 MHz LTS/HTS NMR magnet, while Fig. 7(d) shows a projection of the spectrum. The general shape of the projection of the spectrum coincides well between the two magnets, although six peaks indicated by the arrow in Fig. 7(b) are missing in Fig. 7(d); they appeared if the contour threshold was

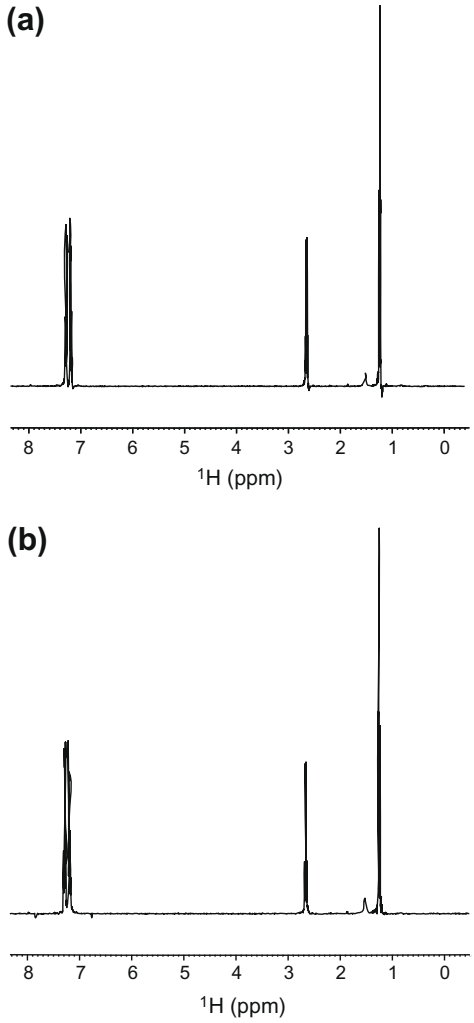

Fig. 5. ^{1}H sensitivity for 0.1% ethylbenzene in $CDCL_3$ with a sample rotation of 20 Hz. The spectrum was obtained by a single scan. (a) Spectrum obtained by a 500 MHz LTS NMR magnet and (b) spectrum by the 500 MHz LTS/HTS NMR magnet.

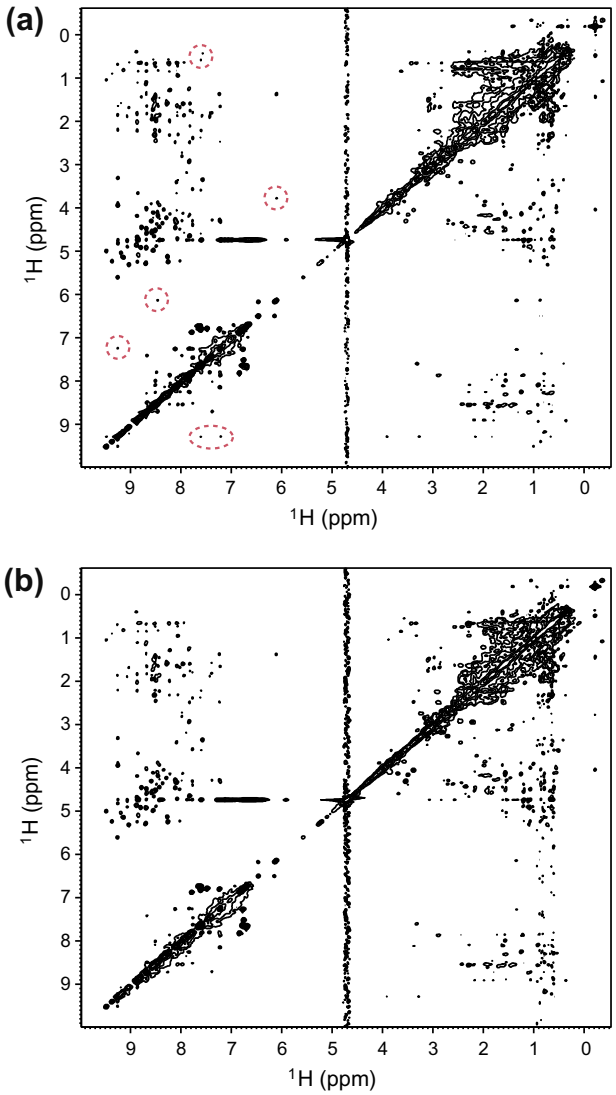

Fig. 6. WATERGATE NOESY spectrum for 2 mM ^{13}C- and ^{15}N-labeled chlorella ubiquitin in 90% H_2O and 10% D_2O obtained by (a) a conventional 500 MHz LTS NMR magnet and (b) the 500 MHz LTS/HTS NMR magnet. The mixing time for NOESY was 0.2 s and the repetition time was 1 s. The number of signal points along the t_2 axis was 1024, while that along the t_1 axis was 512. Number of scans was 16. The acquisition time was 3 h.

lowered. Thus, the data clearly demonstrate that the 3D NMR spectra from proteins can be achieved by the 500 MHz LTS/HTS NMR spectrometer operated in external current mode. The 3D-HNCO spectrum for the same sample was also achieved by the LTS/HTS NMR spectrometer.

4. Discussion

4.1. Effect of screening current-induced magnetic field on the magnetic field stability

The temporal change in the screening current-induced magnetic field has been simulated for a Bi-2223 inner solenoid under the magnetic field generated by LTS outer solenoids. Details of the calculation are given in Ref. [22] and are only briefly described here. A solenoid is modeled as M sets of superconducting concentric coil-rings; each coil-ring corresponds to one turn. The screening current is induced in each turn by a radial component of the magnetic field, generated by the NMR coils. The motion of the screening current density in each turn induced by arbitrary coil current sweep is numerically simulated, based on the simulation method proposed by Brandt [23] and Yazawa et al. [24]. The vertical width of the Bi-2223 tape is discretized into $2N$ points, while its thickness is not discretized. The equations of motion of the screening current density at each discretized point for coil-rings are simultaneously solved for each time step, and then the current densities for all discretized points are obtained. The normal transition voltage for an HTS tape is given by the power law of the critical current [24]. The temporal change of the central magnetic field by screening current is numerically calculated by using elliptic integrals of the first and second kinds, based on the total amount of the central magnetic field generated by each of the discretized points.

Fig. 8 shows the simulated screening current-induced magnetic field profile at $t = 0$ h along the coil axis at the operation current of 144 A; the blue-dashed line shows a magnetic field for the 500 MHz LTS/HTS NMR magnet, while the solid line shows that for the Bi-2223 inner solenoid alone. The magnetic field intensity for Bi-2223 coil seen in Fig. 8 is dominated by the screening currents concentrated at the coil ends and therefore it shows a positive peak at 190 mm, while the field intensity exhibits a negative peak at the coil center. As the HTS critical current density for the LTS/HTS 500 MHz magnet is smaller than that for a Bi-2223 inner

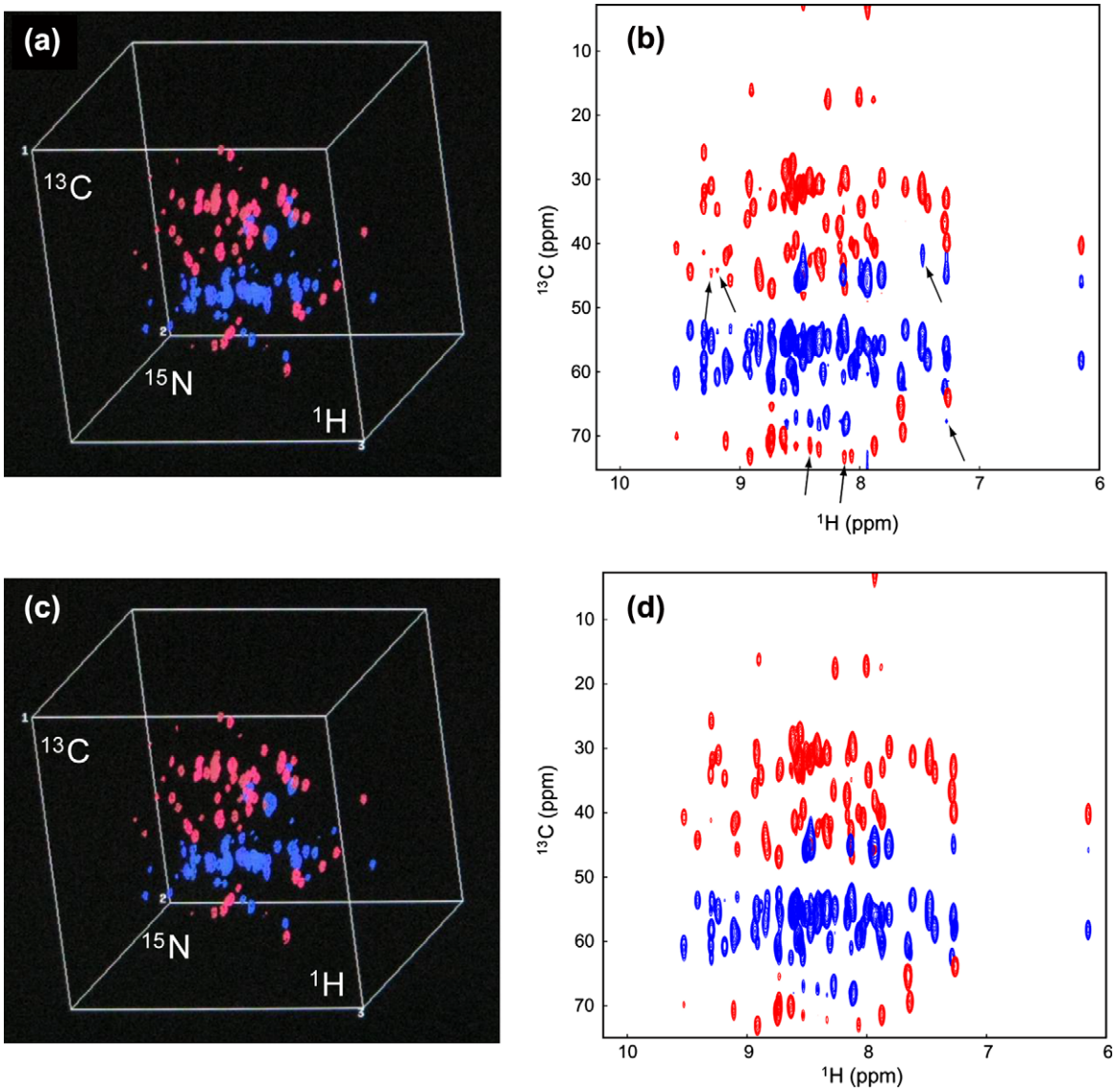

Fig. 7. HNCACB spectra for 2 mM ^{13}C- and ^{15}N-labeled chlorella ubiquitin in 90% H_2O and 10% D_2O. The number of signal points along the t_3 (^{1}H) axis, t_2 (^{13}C) axis, and t_1 (^{15}N) axis were 1024, 64, and 32, respectively. Number of scans was 16. The repetition time was 1 s and the acquisition time 10 h. (a) 3D-HNCACB spectrum obtained by the 500 MHz LTS NMR magnet. (b) A projection of the 3D-HNCACB spectrum from the ^{13}C-^{1}H aspect obtained by a 500 MHz LTS NMR magnet. (c) 3D-HNCACB spectrum obtained by the 500 MHz LTS/HTS NMR magnet. (d) A projection of the 3D-HNCACB spectrum from the ^{13}C-^{1}H aspect obtained by the 500 MHz LTS/HTS NMR magnet.

solenoid alone, the screening current-induced magnetic field intensity for the LTS/HTS 500 MHz NMR magnet, shown by the broken line, is smaller than that for the Bi-2223 solenoid alone, shown by the solid line. For the LTS/HTS 500 MHz NMR magnet, the negative peak collapses around the coil center, due to the effect of radial magnetic field generated by the field correction coils. The geometrical shape of the field correction coil of an NMR magnet is shown in Ref. [25]. The central peak is −56.27 G corresponding to 479.3 ppm (i.e. 239.7 kHz). If the relaxation rate is large, the magnetic field decays steeply and it is improbable that we can make a long-term NMR measurement. Fortunately, the relaxation is slow and shows a logarithmic time dependence as seen in Fig. 1(inset), and therefore it becomes sufficiently small within several weeks for this LTS/HTS NMR magnet.

Relaxation in negative magnetic field at the coil center seen in Fig. 8 results in positive drift of the central magnetic field as seen in Figs. 1 and 2 [15,22]. Fig. 9 shows such a positive drift of the screening current-induced magnetic field intensity after the coil charge. The experimental results for the Bi-2223 inner coil alone, shown by the black-solid line, and those for the 500 MHz LTS/HTS NMR magnet, shown by the blue solid line, agree well with the numerical simulations shown by the black broken line and the blue broken line, respectively. Thus it is demonstrated that the positive drift after the charge of the magnet is due to relaxation of the screening current-induced magnetic field; relaxation in screening current is due to creep of the trapped magnetic flux inside the Bi-2223 tape, referred to as flux creep [19]. As the central screening current-induced magnetic field for the 500 MHz LTS/HTS NMR is 10× smaller than that for the Bi-2223 inner coil alone due to the effect of the field correction coils, as seen by Fig. 8, the drift rate for the NMR magnet is one-third of that for the Bi-2223 inner coil alone.

4.2. Effect of current sweep reversal on the field stability

In a previous paper, we demonstrated that the positive drift of the apparent magnetic field seen in Fig. 1 is sufficiently stabilized if we use a "current sweep reversal technique" when we charge the

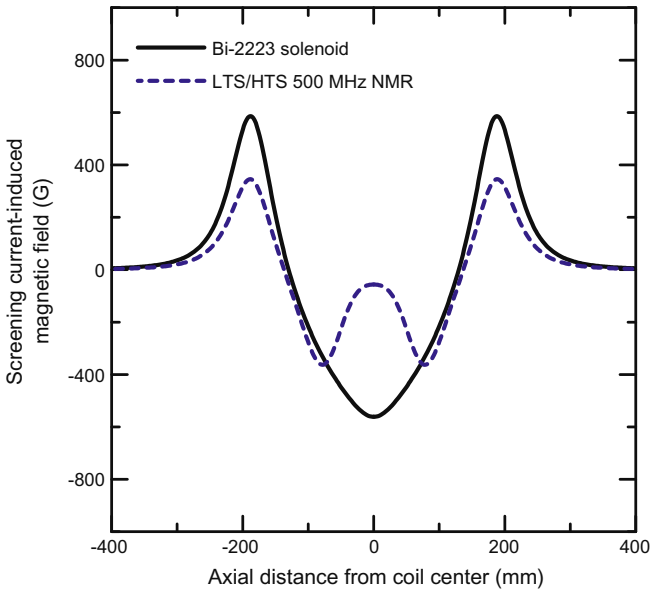

Fig. 8. The simulated screening current-induced magnetic field profile at $t = 0$ h along the coil axis at 144 A; the blue-dashed line shows a magnetic field for the 500 MHz LTS/HTS NMR magnet, while the solid line shows that for the Bi-2223 inner solenoid alone. (For interpretation of the references to color in this figure legend, the reader is referred to the web version of this article.)

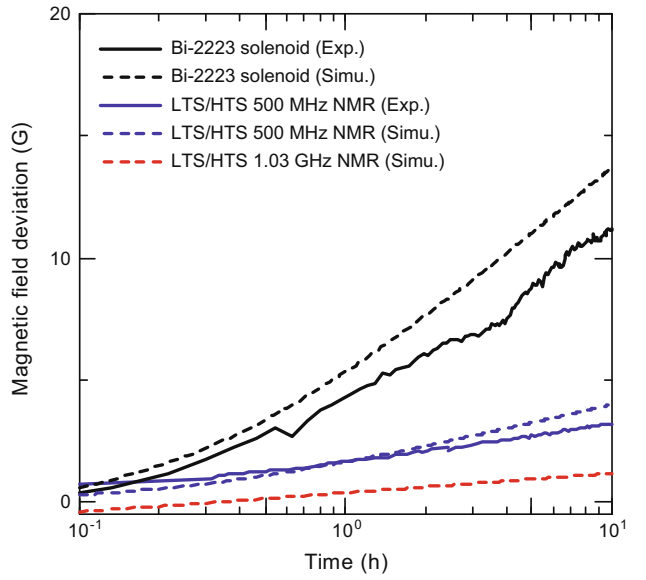

Fig. 9. Positive drift of the screening-current-induced magnetic field intensity after the coil charge. The experimental results for the Bi-2223 inner coil alone, shown by the black-solid line, and those for the 500 MHz LTS/HTS NMR magnet, shown by the blue solid line, agree well with the numerical simulations shown by the black broken line and the blue broken line, respectively. The red dashed line shows a simulated drift for the 1.03 GHz LTS/HTS NMR magnet.

NMR magnet [22]; i.e. the current sweep is reversed by a few % at a peak current, which produces barriers against flux entrance into the Bi-2223 tape from the top and bottom ends of the conductor. The current sweep reversal technique was applied to the second charging experiment of the 500 MHz LTS/HTS NMR, where the coil current was swept to 145.162 A and then discharged quickly to 143.725 A. The blue broken line in Fig. 1 shows the experimental result. The effect of current sweep reversal is dramatic and the magnetic field is nearly constant soon after its coil charge. Thus, it is demonstrated that the field drift due to screening current-induced field is stabilized by the current reversal technique.

4.3. Temporal change of the z and z^2 field gradients

We made a long-term NMR measurement on 1% $CHCl_3$ in acetone-d_6 using the LTS 500 MHz NMR; the line width deteriorated to several Hz in 20 h. The deterioration was suppressed if we used the autoshim feature with z and z^2 shims. The temporal change in the control-signal of the shim current under continuous operation of autoshim over 20 h for a LTS NMR magnet is shown in Fig. 10; Fig. 10(a) shows that for the z shim and Fig. 10(b) that for the z^2 shim. The results were obtained by NMR measurement of 1% $CHCl_3$ in acetone-d_6. The change in z control-signal corresponds to a line broadening of 3.0 Hz and the change in z^2 control-signal to 2.0 Hz. On the other hand, temporal change in the z shim control-signal (see Fig. 10(c)) and that of the z^2 shim (see Fig. 10(d)) for the LTS/HTS NMR magnet was 2.3 and 1.6 Hz respectively. It is clear that temporal changes in z gradient and z^2 gradient were nearly the same between the LTS NMR and the LTS/HTS NMR. A particular point of interest for the LTS/HTS NMR magnet is the gradual growth in y gradient with time, which may have been due to radially unsymmetric relaxation of the screening current. Further investigation of this behavior is required.

4.4. Towards beyond-1 GHz NMR

To operate beyond 1 GHz with a LTS/HTS NMR in external current mode, the permissible peak–peak amplitude of the field fluctuation is one half of the 500 MHz NMR, i.e. 1.5×10^{-6} (1.5 ppm), as the NMR magnetic field intensity is double that of the 500 MHz NMR. However, according to Fig. 2, peak-peak amplitude of the field fluctuation caused by the ultra-stabilized DC power supply is <0.4 ppm, and therefore it is possible to fully stabilize the DC power supply fluctuation by the ^{2}H field-frequency lock system.

The positive magnetic field drift after the coil charge for the 1.03 GHz NMR was numerically simulated, and the results are shown by the red dashed line in Fig. 9.[1] The numerical simulation assumed the following design of the Bi-2223 inner coil for the 1.03 GHz LTS/HTS NMR magnet: 78.4 mm in inner diameter, 122.68 mm in outer diameter, and 838 mm in coil height. The magnetic field drift rate was threefold smaller than that for the 500 MHz NMR magnet, due to (1) a higher radial magnetic field generated by the field correction coils near the coil center, and (2) a larger distance from the coil ends, where the screening current was concentrated, to the coil center for the Bi-2223 coil of the 1.03 GHz NMR magnet. Based on the numerical simulation, the magnetic field drift rate for the 1.03 GHz NMR will attain 10^{-8} (0.01 ppm)/h in a few weeks after the coil charge. If we use the current reversal technique, the time interval will be shortened.

NMR spectra seen in Fig. 4 are modulated by mechanical vibrations especially in the case of a GM cryocooler, while if we use a pulse-tube cycle cryocooler, mechanical vibration is greatly reduced. We are investigating an optimal cryostat design for the beyond-1 GHz LTS/HTS NMR magnet operated in external current mode with and without a cryocooler.

5. Conclusions

(a) The temporal magnetic field drift of the 500 MHz LTS/HTS NMR magnet after the coil charge is dominated by relaxation of the screening current in the Bi-2223 tape; its temporal change rate rapidly reduces with time and reaches 10^{-8} (0.01 ppm)/h at the 20th day. As it is as small as the persis-

[1] For interpretation of color in Fig. 9, the reader is referred to the web version of this article.

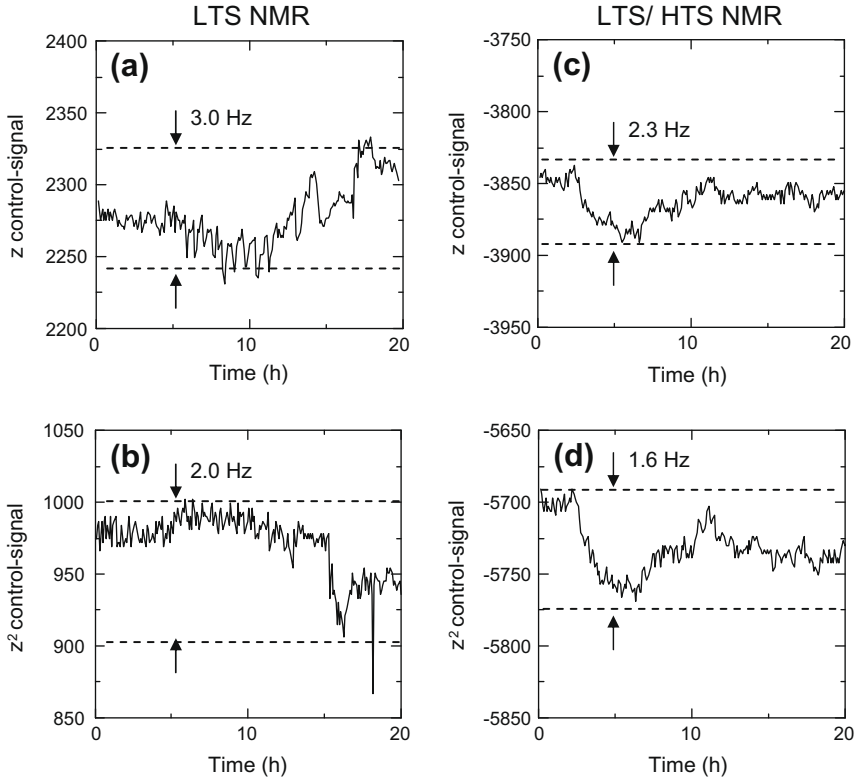

Fig. 10. Temporal change in (a) z shim control-signal and (b) z^2 shim control-signal for a 500 MHz LTS NMR magnet. Temporal change in (c) z shim control-signal and (d) z^2 shim control-signal for the 500 MHz LTS/HTS NMR magnet.

tent current mode NMR magnet, we can fully operate the ^{2}H field-frequency lock system.

(b) Positive magnetic field drift with time after the coil charge is sufficiently stabilized by the current sweep reversal technique.

(c) The 1D ^{1}H NMR spectra obtained by the 500 MHz LTS/HTS magnet is nearly equivalent to those obtained by the LTS NMR magnet operated in persistent current mode. If we use a GM cryocooler installed on top of the cryostat, the NMR spectra is modulated by mechanical vibration of the magnet. The modulation is sufficiently suppressed if we use a pulse-tube type of cryocooler, which induces much less mechanical vibration on the magnet.

(d) The 2D-NOESY, 3D-HNCO, and 3D-HNCACB spectra have been achieved for ^{13}C- and ^{15}N-labeled chlorella ubiquitin by the 500 MHz LTS/HTS magnet; the general shapes of the spectra obtained by the 500 MHz LTS/HTS NMR magnet coincide well with those obtained by a 500 MHz LTS NMR magnet, although the former's signal intensities are slightly lower and t_1 noises are slightly larger than those obtained with the 500 MHz LTS NMR magnet.

(e) Based on a numerical simulation, the effect of screening current-induced magnetic field is harmless for the 1.03 GHz NMR magnet system.

Acknowledgments

This work is supported by SENTAN, JST in Japan.

References

[1] Andrew E. Derome, Modern NMR techniques for Chemistry Research, Pergamon Press, 1987.
[2] K. Pervushin, R. Riek, G. Wider, K. Wüthrich, Attenuated T_2 relaxation by mutual cancellation of dipole–dipole coupling and chemical shift anisotropy indicates an avenue to structures of very large biological macromolecules in solution, Proc. Natl. Acad. Sci. USA 94 (1997) 12366–12371.
[3] Z. Gan, P. Gor'kov, T.A. Cross, A. Samson, Dominique Massiot, Seeking higher resolution and sensitivity for NMR of quadrupolar nuclei at ultra high magnetic fields, J. Am. Chem. Soc. 124 (2002) 5634–5635.
[4] <http://www.bruker-biospin.com/pr090601.html>.
[5] S. Hong, M.B. Field, Jeffrey A. Parrell, Y. Zhang, Latest improvements of current carrying capability of niobium tin and its magnet applications, IEEE Trans. Appl. Supercond. 16 (2006) 1146–1151.
[6] A.J. Varney, NMR in Mechanistic Systems Biology, 2009, pp. 101–104. Available from: <http://www.postgenomicnmr.net/NMRLife/docs/NMR_in_MSB.pdf>.
[7] K. Ohkura, K. Sato, M. Ueyama, J. Fujikami, Y. Iwasa, Generation of 24.0 T at 4.2 K and 23.4 T at 27 K with a high-temperature superconductor coil in a 22.54 T background field, Appl. Phys. Lett. 13 (1995) 1923–1925.
[8] H.W. Weijers, U.P. Trociewitz, K. Marken, M. Meinesz, H. Miao, J. Schwartz, The generation of 25.05 T using a 5.11 T $Bi_2Sr_2CaCu_2O_x$ superconducting insert magnet, Supercond. Sci. Technol. 17 (2004) 636–644.
[9] D.W. Hazelton, V. Selvamanickam, J.M. Duval, D.C. Larbalestier, W.D. Markiewitcz, H.W. Weijers, R.L. Holtz, Recent development in 2G HTS coil technology, Presented to the Appl. Super. Conf., vol. 3LY01, 2008.
[10] T. Kiyoshi, A. Otsuka, S. Choi, S. Matsumoto, K. Zaitsu, T. Hase, M. Hamada, M. Hosono, M. Takahashi, T. Yamazaki, H. Maeda, NMR upgrading project towards 1.05 GHz, IEEE Trans. Appl. Supercond. 18 (2008) 860–863.
[11] Y. Yanagisawa, H. Nakagome, M. Hoshino, M. Hamada, T. Kiyoshi, F. Hobo, M. Takahashi, T. Yamazaki, H. Maeda, Towards beyond-1 GHz solution NMR: internal ^{2}H lock operation in an external current mode, J. Mag. Res. 192 (2008) 329–337.
[12] T. Kiss, M. Inoue, T. Kuga, M. Ishimaru, S. Egashira, S. Irie, T. Ohta, K. Imamura, M. Yasunaga, M. Takeo, T. Matsushita, Y. Iijima, K. Kakimoto, T. Saitoh, S. Awaji, K. Watanabe, Y. Shiohara, Critical current properties in HTS tapes, Physica C 392–396 (2003) 1053–1062.
[13] Y. Yanagisawa, H. Nakagome, M. Hosono, M. Hamada, T. Kiyoshi, F. Hobo, M. Takahashi, T. Yamazaki, H. Maeda, Towards beyond-1 GHz NMR: field stabilization and NMR measurement in the external current mode, in: Proceedings of ICEC 22 – ICMC 2008, 2009, pp. 853–858.
[14] S. Hahn, J. Bascunan, W. Kim, E.S. Bobrov, H. Lee, Y. Iwasa, Field mapping, NMR lineshape, and screening current induced field analyses for homogeneity improvement in LTS/HTS NMR magnets, IEEE Trans. Appl. Supercond. 18 (2008) 856–859.
[15] Y. Koyama, T. Takao, Y. Yanagisawa, H. Nakagome, M. Hamada, T. Kiyoshi, M. Takahashi, H. Maeda, Towards beyond 1 GHz NMR: mechanism of the long term drift of screening current-induced magnetic field in a Bi-2223 coil, Physica C 469 (2009) 694–701.

[16] T. Kiyoshi, S. Choi, S. Matsumoto, K. Zaitsu, T. Hase, T. Miyazaki, A. Otsuka, M. Yoshikawa, M. Hamada, M. Hosono, Y. Yanagisawa, H. Nakagome, M. Takahashi, T. Yamazaki, H. Maeda, HTS-NMR: present status and future plan, IEEE Trans. Appl. Supercond., to be published.
[17] <http://www.danfysik.com/documents/Fact_Sys8500_MPS854_0605_A.pdf>.
[18] R. Otsuka, T. Kiyoshi, S. Matsumoto, K. Kominato, M. Takeda, Filed stability of a 600 MHz NMR magnet in the driven-mode operation, IEEE Trans. Appl. Supercond. 18 (2008) 852–855.
[19] Y. Yeshurun, A.P. Malozemoff, A. Shaulov, Magnetic relaxation in high-temperature superconductors, Rev. Modern Phys. 68 (1996) 911–949.
[20] T.D.W. Claridge, High-Resolution NMR Techniques in Organic Chemistry, Elsevier, 1999. p. 168.
[21] K. Tennmei, Y. Yanagisawa, H. Nakagome, M. Hamada, A. Otuka, T. Kiyoshi, M. Takahashi, H. Maeda, Relation between characteristic of vibration spectra and NMR for signal of 500 MHz LTS/HTS NMR – towards an NMR spectrometer beyond 1 GHz, in: 50th Experimental Nuclear Magnetic Resonance Conference, 2009, PS, p. 491.
[22] Y. Yanagisawa, H. Nakagome, Y. Koyama, R. Hu, T. Takao, M. Hamada, T. Kiyoshi, M. Takahashi, H. Maeda, Effect of current sweep reversal on the magnetic field stability for a Bi-2223 superconducting solenoid, Physica C 469 (2009) 1996–1999.
[23] E.H. Brandt, Thin superconductors in a perpendicular magnetic ac field: general formulation and strip geometry, Phys. Rev. B 49 (1994) 9024–9040.
[24] T. Yazawa, J.J. Rabbers, B. ten Haken, H.H.J. ten Kate, Y. Yamada, Numerical calculation of current density distributions in high temperature superconducting tapes with finite thickness in self field and external field, Physica C 310 (1998) 36–41.
[25] Y. Iwasa, Case Studies in Superconducting Magnets-Design and Operational Issues, Plenum Press, New York, 1994. p. 362.